World Conference on Timber Engineering Oslo 2023

SIZE EFFECT OF LARGE GLUED LAMINATED TIMBER BEAMS – CONTRIBUTION TO THE ONGOING DISCUSSION

Christoffer Vida[1], Markus Lukacevic[2], Georg Hochreiner[3], Milena Stavric[4], Josef Füssl[5]

ABSTRACT: The effort to experimentally test glued laminated timber (GLT) beams is tremendous, especially for large beams. Such beams are increasingly used to realise wide-span timber structures, but experimental investigations of large beams are missing. In the literature, numerical simulation studies can be found instead to estimate the influence of the beam size. However, these studies come to partly different conclusions regarding the size effect, which confirms the high influence of the modelling strategy. Therefore, we conducted an extensive simulation program covering more than 8000 simulations to research the size effect, including large GLT beams of up to 3300 mm depth.

The developed modelling concept considered the morphology of timber boards deterministically and accounts for discrete cracking to simulate the bending strengths of GLT beams subjected to four-point bending tests. We predicted the size effect on the characteristic bending strength for two commonly used strength classes. We found that the strength decreased with increasing beam size. The results showed that the strength decrease is not only caused by the beam depth but also the length. Furthermore, the influence of different global failure criteria was investigated, with which the results from the existing studies could successfully be reproduced.

KEYWORDS: Glued laminated timber, XFEM, Size effect, Global failure criterion

1 INTRODUCTION

Glued laminated timber (GLT) is a building material suitable to realise a large variety of wide-span structures, e.g., hall constructions as well as office or apartment buildings. In recent decades, the dimensions, especially the beam depth, of GLT beams have increased continuously. The versatile use of GLT requires a comprehensive understanding of the mechanical behaviour and effective properties of the material. However, there is a debate among experts about the influence of the size of GLT beams on their bending strength.

This so-called size effect on the characteristic bending strength $f_{\mathrm{b,k}}$ can be described by applying the commonly used factor k_{h} to a characteristic reference bending strength $f_{\mathrm{b,k,ref}}$:

$$f_{\mathrm{b,k}} = f_{\mathrm{b,k,ref}} \cdot k_{\mathrm{h}} \,. \tag{1}$$

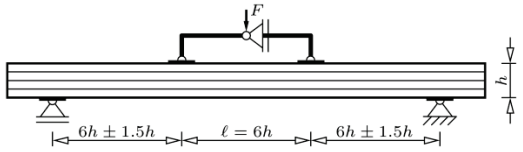

Figure 1: *Four-point bending test setup for a GLT beam according to DIN EN 408 [1] with the depth h and length ℓ.*

According to DIN EN 1995-1-1 [2], $f_{\mathrm{b,k,ref}}$ is provided in DIN EN 14080 [3] ($f_{\mathrm{m,g,k}}$) for beams with the reference beam depth $h_{\mathrm{ref}} = 600\,\mathrm{mm}$ of individual strength classes. The experimental test setup for GLT beams, according to DIN EN 408 [1], is a four-point bending test (Fig. 1), where the beam length is always proportional to the beam depth. Further, the factor k_{h} in [2] is only applicable for smaller beams, reading:

$$k_h = \min\begin{cases}\left(\dfrac{600}{h}\right)^{0.1} \\ 1.1\end{cases}, \tag{2}$$

with a maximum strength increase that is limited to 10 %.

The power law given in Eq. (2) is consistent with the one for wooden members presented by Bohannan [4] based on Weibull's strength theory [5]. Colling [6] also proposed considering the beam volume V and the loading configuration. Here we focus on the size effect k_{h} based on the volumes that reads as:

$$k_{\mathrm{h}} = \left(\frac{V_{\mathrm{ref}}}{V}\right)^{1/m}, \tag{3}$$

where V_{ref} is the reference Volume.

The effort involved in the experimental testing of larger GLT beams is tremendous. Thus, experimental investigations on the size effect in the literature [7–9] focused on smaller GLT beams with depths up to

[1] Christoffer Vida, TU Wien, Austria, christoffer.vida@tuwien.ac.at
[2] Markus Lukacevic, TU Wien, Austria, markus.lukacivic@tuwien.ac.at
[3] Georg Hochreiner, TU Wien, Austria, goerg.hochreiner@tuwien.ac.at
[4] Milena Stavric, TU Graz, Austria, mstavric@tugraz.at
[5] Josef Füssl, TU Wien, Austria, josef.fuessl@tuwien.ac.at

https://doi.org/10.52202/069179-0063

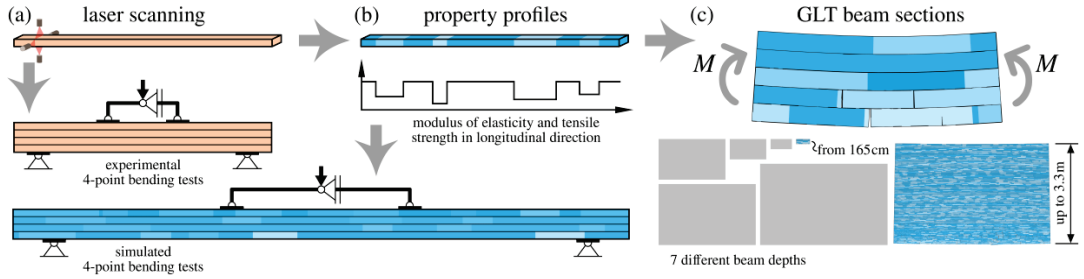

Figure 2: *Modelling concept that was based on (a) GLT beams assembled by real timber boards [8], (b) GLT beams reconstructed by virtual boards using derived material property profiles of real wooden boards [13], and (c) GLT beam sections employed to estimate the size effect [12].*

600 mm. For the larger sizes, numerical studies were conducted, e.g., by Frese and Blaß [10] and Fink et al. [11], covering beam depths up to 3000 mm and 1200 mm, respectively. These studies, however, provided partly contradictory results.

Therefore, we conducted an extensive simulation campaign to study the size effect for beams having depths up to 3300 mm [12]. The applied approach was based on a previous approach that simulates the entire loading process of GLT beams subjected to four-point bending tests [13]. Herein, we present the modelling concept that enabled us to predict the size effect for different beam depths and lengths. Furthermore, global failure criteria similar to the ones used in the literature [10, 11] could be implemented and investigated, which will be presented in detail in [14].

The present paper gives an overview of these studies. The structure is as follows: Section 2 presents the modelling concept to simulate the bending strength of GLT beams subjected to four-point bending tests. The investigation of the size effect and different global failure criteria is presented in Section 3. The paper closes with conclusions and an outlook.

2 MODELLING CONCEPT

The modelling concept builds upon a set of virtual boards to assemble GLT beams (Fig. 2). An experimental study [8] on GLT beams provided the morphological details of real wooden boards based on surface laser scans (Fig. 2a). This enabled the virtual replication of each individual board with deterministic material properties, as outlaid in [15]. The approaches by Frese and Blaß [10] and Fink et al. [11] used, in contrast, stochastic methods to construct the boards and their material properties. Vida et al. [13] presented a modelling approach to simulate the entire loading course of GLT beams subjected to four-point bending tests (Fig. 2b). For the study on the size effect [12], the approach was adjusted to suit the research scope and its efficiency was increased by reducing its model size (Fig. 2c). There, only a beam section anywhere between the two loading points of a four-point bending test was considered, which allowed applying the constant bending moment M directly.

An overview of the procedure deriving the used material properties is presented in Section 2.1. Section 2.2 describes the modelling approach for beam sections before Section 2.3 continues with its validation. The realisation of different beam lengths is discussed in Section 2.4.

2.1 MATERIAL PROPERTIES

The material properties were based on the deterministic estimation procedure presented by Kandler et al. [15]. Therein, the boards were virtually reconstructed and parted in sections. The section length ℓ_s was based on the corresponding knot configuration in the real wooden board, and thus the sections were of individual size (Fig. 3). Each section refers either to defect-free wood, so-called clear wood, or to sections with single large knots or knot clusters, referred to as knot sections.

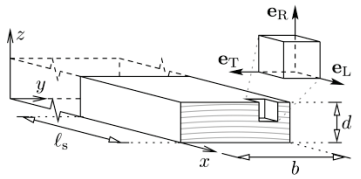

Figure 3: *Board section with homogeneous material properties. [13]*

The material properties of each section were constant, and the material behaviour was orthotropic. The stiffness properties for the clear wood sections were based on a micromechanical multiscale model proposed by Hofstetter et al. [16]. The model used density and moisture content as the primary input parameters. Consequently, each board had its own individual stiffness tensor $\mathbb{C}$. A separate FE approach [15] estimated the longitudinal modulus of elasticity (MOE) $E_{L,i}$ for each knot section i individually. The stiffness tensor $\mathbb{C}$ was then modified along the board by $E_{L,i}$. The tensile strength in longitudinal direction $f_{t,i}$ was assumed to be $55\ \mathrm{N/mm^2}$ for the clear wood sections of all boards. However, the clear wood strength represents an upper strength limit having only a minor influence on the load-bearing capacity [13]. Within knot sections, $f_{t,i}$ was estimated by the knot-area ratio according to the study presented by Lukacevic et al. [17]. Finally, the section-wise constant effective MOE $E_{L,i}$ and tensile strength $f_{t,i}$ in the longitudinal direction were provided for each board by two material property profiles (Fig. 4a,d). Two strength classes, T14 and T22, were considered.

https://doi.org/10.52202/069179-0063

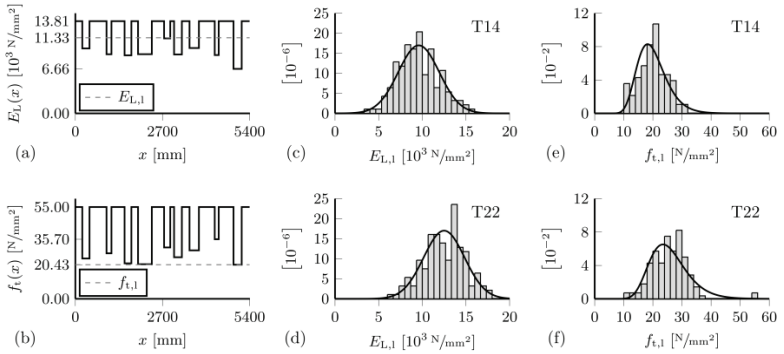

Figure 4: *Example of a board's property profiles providing (a) the effective longitudinal MOE $E_L(x)$ and (b) the effective tensile strength $f_t(x)$ as well as histograms considering all boards and PDFs fitted by maximum likelihood estimations for (c,d) the MOE $E_{L,l}$ and (e,f) the tensile strengths $f_{t,l}$, separate for both strength classes T14 and T22. [13]*

In total, 140 boards of each strength class were available. The board's length was 5400 mm, the width 90 mm, and the thickness 33 mm. The longitudinal MOE of an entire board $E_{L,l}$ considered all sections i of the board as a chain of linear springs:

$$E_{L,l} = \frac{\ell_{tot}}{\sum_i \frac{\ell_{s,i}}{E_{L,i}}} \quad \text{with} \quad \ell_{tot} = \sum_i \ell_{s,i}\,, \tag{4}$$

where $\ell_{s,i}$ is the length corresponding to the section-wise constant $E_{L,i}$ from its stiffness profile (Fig. 4a). Figure 4c,d shows the histograms and the fitted normal probability distribution functions (PDFs) of $E_{L,l}$ according to Eq. (4) for both strength classes T14 and T22, respectively. The board tensile strength $f_{t,l}$ is assumed as the lowest strength $f_{t,i}$ of section i within the strength profile of the considered board (Fig. 4b):

$$f_{t,l} = \min_i \{f_{t,i}\}\,. \tag{5}$$

Figure 2e,f shows the histograms and the fitted log-normal PDFs of $f_{t,l}$ according to Eq. (5) again for both strength classes, respectively. A comparison of the characteristic tensile board strength and the mean longitudinal board MOE to the values according to DIN EN 14080 [3] is given in Tab. 1. Generally, the simulated values are lower than those specified in the standard. The underestimation could be due to different board lengths in the test setup, especially regarding the strengths.

2.2 MODELLING APPROACH

We used a non-linear FE approach to simulate GLT beam sections (Fig. 5) by employing the FE software Abaqus [18]. Details about the approach are published in [12]. The beam layout was assembled by the virtually reconstructed boards from Section 2.1, and the beam structure was designed to be homogeneous. Consequently, only boards corresponding to strength class T14 or T22 were used to simulate beams of strength class GL 24h or GL 30h, respectively. The boards within a beam were arranged by a uniformly distributed pseudo-random process of the following steps:

1. Random picking a full-length board from the entire pool of virtual boards.
2. Random longitudinal displacement of the board within the GLT beam section to define the start and end positions of the lamella.
3. Random choice of the lamella's orientation in the GLT beam layout.

Typically, restrictions on the length of boards are reversed by connecting individual boards with finger joints. Herein, weak points due to finger joints were neglected. We assumed that the structural behaviour and failure is covered by the random allocation of natural weak spots, as it was found by experimental studies [7, 19].

The beam section (Fig. 5) was modelled with the variable length-to-depth ratio ℓ/h, where $h = k \cdot 33$ mm depending on the number of laminations k. The length $e = 100$ mm was added on both ends to avoid disturbing the area of interest by load application effects. The constant bending moment M was applied at the reference points R_1 and R_2 by prescribing a reversed rotation. During the loading, the cross-sections at both beam ends stayed planar. The beam width b was according to the used boards, and the symmetry in the

Table 1: *Comparison of the mean and characteristic values of the histograms in Fig. 2c–f to values according to DIN EN 14080 [3]. [13]*

Strength class	$E_{L,l,mean}$ (N/mm²)	$E_{L,0,l,mean}$ (N/mm²)	$f_{t,0,l,k}$ (N/mm²)	$f_{t,0,l,k}$ (N/mm²)
T14	9 592	11 000	11.6	14.0
T22	12 497	13 000	16.6	22.0

https://doi.org/10.52202/069179-0063

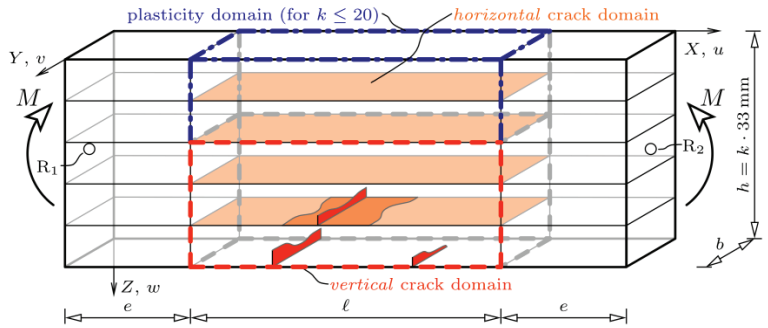

Figure 5: *Representative GLT beam section of length ℓ as used for the numerical simulations with k lamellas resulting in the depth h. The constant bending moment M and the bearing were applied at the reference points R_1 and R_2. [12]*

width direction was exploited to reduce the model size further.

We considered different kinds of local failure mechanisms within the approach, i.e., discrete cracks in the vertical and horizontal direction as well as plastic deformations. All failure mechanisms could only take place within the region of the length ℓ as marked in Fig. 5.

The vertical cracks could occur within the lamellas on the tensile side, and the horizontal cracks between all adjacent laminations building up the beam section (Fig. 5). Both crack directions enabled the formation of a continuous crack over multiple laminations. Two vertical cracks with a horizontal offset and in adjacent laminations could be connected by a horizontal crack. Their implementation is briefly outlined in the following:

- *Vertical* cracks were realised within the framework of XFEM, which was proposed by Tapia Camú and Aicher [20]. The application of XFEM enabled an element to split into two parts with planar and opposing crack surfaces. The split was initiated by an initiation criterion, i.e., the tensile stress in the centroid of an element exceeding the tensile strength $f_{t,i}$. The maximum traction stress t^* between the crack surfaces was, thus, $f_{t,i}$. A linear traction–separation (t–δ) law (Fig. 6a) governed the interaction between the crack surfaces in conjunction of a constant fracture energy $G_{f,v} = 30\ \mathrm{Nmm/mm^2}$.
- *Horizontal* cracks were implemented with cohesive surfaces. The traction–separation (t–δ) relation between the two parts was linear elastic until the initiation of damage and its evolution (Fig. 6b). The maximum traction stress t^* is set to $5.0\ \mathrm{Nmm/mm^2}$ and $6.0\ \mathrm{Nmm/mm^2}$ for transversal tensile stresses and shear stresses, respectively. An uncoupled stiffness tensor defined the traction t between the surfaces and their separation δ. A constant fracture energy $G_{f,h} = 0.6\ \mathrm{Nmm/mm^2}$ was used.

The applied constant properties were assumed because of the lack of available data, e.g., for the fracture energies.

The plastic deformations in compressive zones were considered by implementing ideal plastic behaviour with a multisurface failure criterion [21–23]. The relevance of plastic deformations on the load-bearing capacity was assumed to be limited to smaller beam depths based on an experimental study [8]. Thus, ideal plasticity was only implemented for beams consisting of a maximum of 20 lamellas corresponding to a depth of 660 mm (Fig. 5).

The applied global failure criterion determined the load-bearing capacity M_{max} by the first load decline of at least 3 % from the so far maximum total load M. Finally, the calculated bending strength of the beam reads as:

$$f_b = \frac{6\,M_{max}}{bh^2}, \tag{6}$$

where the dimensions b and h can be found in Fig. 5.

Next is the validation of the approach. The influence of the element size and the plastic deformations on the bending strength are additionally discussed in [12].

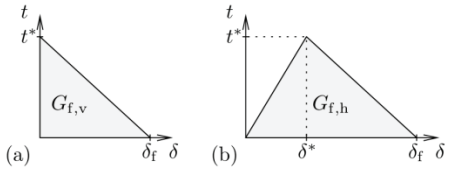

Figure 6: *Traction–separation (t–δ) law with the area representing the fracture energy G_f for (a) vertical cracks and (b) horizontal cracks, where t^* and δ^* are the traction and separation at damage initiation, respectively, and δ_f is the separation at fully evolved damage. [13]*

2.3 VALIDATION

To validate the approach, we compared the results of 40 tested GLT beams with simulation results, i.e., the effective MOE E_{GLT} and bending strength f_b (Fig. 7). The experimental study [8] focused on GLT beams with well-known knot morphology without containing any finger joints. The beams were manufactured using the same boards from the virtual reconstruction process presented in Section 2.1. Thus, it was possible to recreate each tested beam with the unique beam layout and material properties for the simulations.

The validation covered two strength classes, i.e., GL 24h and GL 30h, and two beam sizes with 132 mm and 330 mm depth. The different beam configurations were classified by four types, A, B, D, and E, designated according to their strength class and number of lamellas:

https://doi.org/10.52202/069179-0063

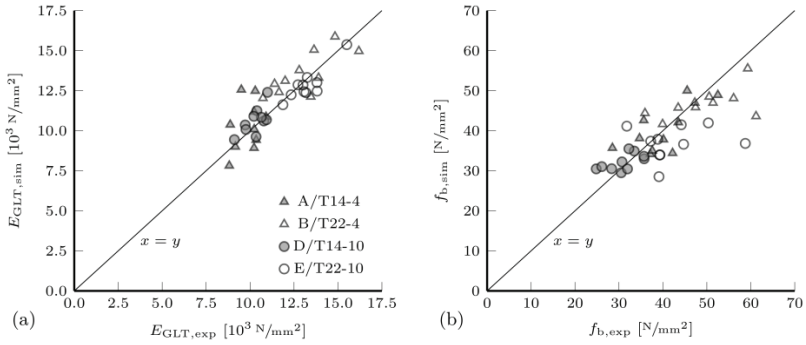

Figure 7: *Comparison of experimental results (subscript exp) to simulation results (subscript sim) for (a) the effective MOE E_{GLT} and (b) bending strength f_b. [12]*

A/T14-4, B/T22-4, D/T14-10, and E/T22-10. The test setup of the experiments was according to DIN EN 408 [1].

The simulations reconstructed the tested beams in the range between the two loading points with a dimensional ratio $\ell/h = 6.0$. The simulation results successfully reproduced the characteristics of the experimental results for the different strength classes and beam sizes, as shown in Fig. 7.

2.4 CONSIDERATION OF DIFFERENT DIMENSIONAL RATIOS

The ratio of beam length to depth ℓ/h, also referred to as dimensional ratio, influences the structural response, as presented in [12]. This was shown by simulating beam sections having ratios ℓ/h of 6.0 and 1.5 for beam depths of h of 165 mm, 330 mm, and 660 mm. However, the larger dimensional ratio requires larger finite element models for which the computation time of the nonlinear calculations became quite long. Therefore, the bending strength prediction of different dimensional ratios based on models having only a ratio of $\ell/h = 1.5$ would be very valuable.

The applied solution to this problem was to estimate the bending strength of larger dimensional ratios $p \times 1.5$ in the following way:

$$f_{b,i} = \min\left\{f_{b,(i-1)\cdot p+1}, f_{b,(i-1)\cdot p+2}, \cdots, f_{b,(i-1)\cdot p+p}\right\}, \quad (7)$$

with $i \in \{1, \ldots, \lfloor n/p \rfloor\}$, where n denotes the number of simulation results from models with $\ell/h = 1.5$ and $\lfloor\cdot\rfloor$ is the floor function that rounds the included number to the nearest smaller integer.

A rough validation was done by comparing the PDFs (Fig. 8) corresponding to the simulation results having the ratio ℓ/h of 6.0 and 4×1.5. The PDFs of f_b were log-normal distributions fitted by maximum likelihood estimations. Considering the simplicity of Eq. (7), the agreement with the simulation results was surprisingly good. The maximum deviation of the mean bending strength was 3.3 % and of the characteristic bending strength 2.2 %. Consequently, the influence of different dimensional ratios can be estimated by this method.

3 COMPUTATIONAL STUDY ON THE SIZE EFFECT

To study the size effect on the bending strength of large GLT beams, we carried out an extensive simulation campaign that is summarised in the following and presented in detail in [12]. The study covered beam sizes ranging from 165 mm up to 3300 mm for two strength classes, i.e., GL 24h and GL 30h. The number of simulations performed depended on the beam size but was the same for both strength classes (Tab. 2). All simulations were carried out with a dimensional ratio of $\ell/h = 1.5$ using the 140 virtually reconstructed wooden boards of each strength class from Section 2.1.

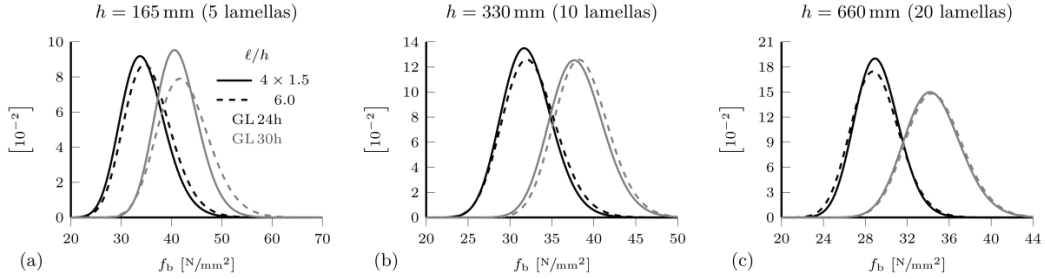

Figure 8: *Comparison of PDFs for the bending strength f_b obtained from simulations with the dimensional ratios of 6.0 or 4×1.5 covering both strength classes for three beam depths: (a) 165 mm, (b) 330 mm, and (c) 660 mm. [12]*

https://doi.org/10.52202/069179-0063

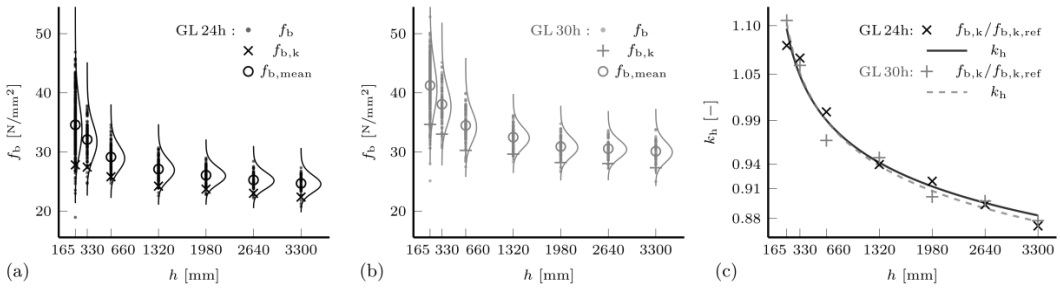

Figure 9: *Bending strength f_b values and PDFs obtained from simulations with the beam depth h and a dimensional ratio of 4 × 1.5 for strength classes (a) GL 24h and (b) GL 30h, which are used to derive (c) the factor k_h commonly used to describe the size effect. [12]*

The study [12] covered GLT beams having fixed dimensional ratios (Section 3.1) and variable dimensional ratios (Section 3.2). Additionally, the influence of the applied global failure criterion was investigated (Section 3.3), and the results will be published in [14].

Table 2: *Studied beam depths with the corresponding number of lamellas and simulations. [12]*

Depth h (mm)	Lamellas k (–)	Sample size[a] (–)
165	5	1600
330	10	400
660	20	400
1320	40	400
1980	60	300
2640	80	200
3000	100	200

[a] For each strength class with $\ell/h = 1.5$

3.1 BEAM SECTIONS WITH FIXED DIMENSIONAL RATIO

The test setup, according to DIN EN 408 [1], always requires a dimensional ratio $\ell/h = 6.0$ for the maximum loaded range. Consequently, the beam length ℓ increases when increasing the depth h. The effective bending strengths were calculated using the simulation results in conjunction with Eqs. (6) and (7) to obtain representative results for the required dimensional ratio $\ell/h = 6.0$.

The effective bending strengths decreased for both strength classes with increasing beam size (Fig. 9a,b). The decrease was present for the mean and characteristic bending strength, $f_{b,mean}$ and $f_{b,k}$, respectively. The mean and characteristic values were obtained from the two-parameter log-normal PDFs, which were fitted to the entire sample by maximum likelihood estimations. Additionally, the PDFs showed a decreasing variation with increasing beam size. The decreasing variation results in a lower decrease of $f_{b,k}$ compared to $f_{b,mean}$.

On the level of $f_{b,k}$, the size effect k_h according to Eq. (3) was clearly present for the entire range of simulated beam sizes (Fig. 9c). For the analytical solution represented by Eq. (3), the characteristic reference bending strength $f_{b,k,ref}$ and the power law parameter m were fitted to the simulation results by the least squares method. The reference depth h_{ref} was set to 600 mm according to DIN EN 14080 [3].

The characteristic reference bending strengths $f_{b,k,ref}$ found through fitting overestimate the values provided in DIN EN 14080 [3] by about 7 % and 4 % for GL 24h and GL 30h, respectively (Tab. 3). The found parameter m is quite similar for both strength classes having a mean value of 26.2.

Both strength classes showed about the same decrease. The largest simulated beams ($h = 3300$ mm) showed a reduced $f_{b,k}$ of about 12 % compared to $f_{b,k,ref}$ (Fig. 9c). For smaller beam depths than h_{ref}, the predicted k_h agrees well with the modification according to Eq. (2) from DIN EN 1995-1-1 [2]. Additionally, our results agreed very well with two experimental studies from the literature testing beams with depths of about 300 mm and 600 mm. Aasheim and Solli [7] and Schickhofer [9] identified k_h as 1.07 and 1.04, respectively. For the same beam depths, our approach predicted k_h to be 1.05. The result was obtained using the mean value of the parameter m corresponding to both strength classes in Eq. (3).

Table 3: *Characteristic reference bending strength $f_{b,k,ref}$ and power law parameter m fitted to the simulation results. [12]*

	GL 24h		GL 30h	
	$f_{b,k,ref}$ (N/mm²)	m (N/mm²)	$f_{b,k,ref}$ (N/mm²)	m (N/mm²)
Load drop	25.74	27.00	31.23	25.38

3.2 BEAM SECTIONS WITH DIFFERENT DIMENSIONAL RATIO

As already pointed out, the test setup, according to DIN EN 408 [1], defines a fixed ratio of the length ℓ between the two loading points and the beam depth h. However, the dimensional ratio ℓ/h of GLT beams is determined during the design process and might not coincide with the fixed dimensional ratio of the experiments. Therefore, investigating the size effect on $f_{b,k}$ for different dimensional ratios ℓ/h is highly relevant for practical application.

https://doi.org/10.52202/069179-0063

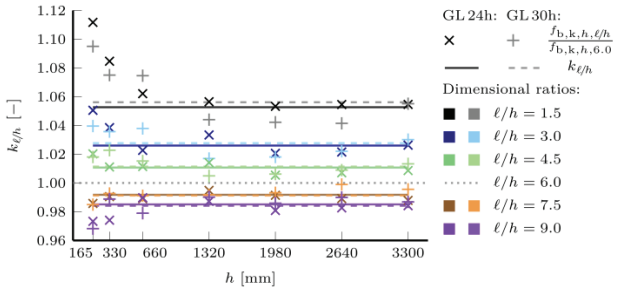

Figure 10: *Comparison of the normalised values $k_{\ell/h}$ of each individual beam depth h: the scatters refer to the simulated results in conjunction with Eq. (7), and the horizontal lines are according to Eq. (3). [12]*

The different ratios ℓ/h were realised using the procedure presented in Section 2.4. The simulation results stemmed from the models having a dimensional ratio of 1.5. For each of the seven simulated beam depths h, five different lengths ℓ were investigated, covering ratios ℓ/h ranging from 1.5 to 9.0. The obtained characteristic bending strengths $f_{b,k,h}$ for each ratio of a specific beam depth h were normalised by $f_{b,k,h,6.0}$ of the same beam depth h with a ratio $\ell/h = 6.0$ (4×1.5). This normalised value is herein denoted as $k_{\ell/h}$.

The simulation results indicated that the ratio ℓ/h heavily influences the bending strength of a GLT beam (Fig. 10). By changing the ratio for a specific beam depth h, the investigated beam length changes. When looking at a particular beam depth, the characteristic bending strength of a beam with a shorter length was smaller than that of a longer length. Especially beams with a depth smaller than 660 mm showed a more pronounced influence of the dimensional ratio ℓ/h. For each individual ratio, the larger beams showed an almost constant factor $k_{\ell/h}$. Consequently, the same size effect is present for only changing the beam length or depth. The horizontal lines in Fig. 10 render the results of Eq. (3) in conjunction with the results provided in Tab. 3. The simulation results agreed well with the analytical concept.

3.3 INFLUENCE OF THE APPLIED GLOBAL FAILURE CRITERION

The applied modelling approach enabled the investigation of different global failure criteria for each simulation. This was possible by simulating the entire loading process and determining the load-bearing capacity afterwards. The size effect on $f_{b,k}$ of large GLT beams had been estimated before by Fink et al. [11] and Frese and Blaß [10]. However, their results diverged from each other. To investigate the influence of applied global failure criteria, we implemented similar criteria within our approach. The modelling strategies of each approach were different, making a completely identical description of the failure criteria impossible, e.g., due to a different mesh size or the implementation of discrete cracking. Nevertheless, we tried to implement the criteria as closely to the proposed one as possible. The implementation of the global failure criteria and the main differences between the modelling strategies will be discussed in detail in [14].

The applied global failure criterion defined the simulated load-bearing capacity M_{max} used to further calculate the corresponding bending strength f_b according to Eq. (6). Additional to our already presented load drop criterion (Section 2.2), we implemented the following global failure criteria:

- The global stiffness reduction criterion is met by the first global stiffness reduction of at least 1 % compared to the initial global stiffness of the first loading increment. The global stiffness is calculated in each increment with the current bending moment and rotation. The load-bearing capacity is then the maximum load during the loading before the criterion is fulfilled. This implementation is similar to the criterion applied by Fink et al. [11].
- The first crack initiation criterion focuses only on the initiation of the first crack in the outermost tensile lamination to identify the load-bearing capacity. The load-bearing capacity is then the maximum bending moment observed during the entire simulation up to this point. During the loading process, an arbitrary number of cracks can occur within the other laminations of the beam. This criterion is comparable with the one used by Frese and Blaß [10] and Frese [24].

The estimated individual trends of the size effect k_h for each global failure criterion (Fig. 11) agreed very well with the results presented in the literature. The stiffness reduction criterion predicted basically no influence of the beam size on $f_{b,k}$, which agrees with the result presented in Fink et al. [11]. The first crack initiation criterion resulted in a decrease only a bit larger than proposed by Frese and Blaß [10]. The characteristic bending strengths of all criteria were taken from fitted log-normal PDFs.

4 CONCLUSION AND OUTLOOK

The development of reliable modelling concepts is of significant importance to effectively investigate wood products such as GLT beams. In the present study, a comprehensive simulation campaign of more than 8000 simulations could predict the size effect for large GLT beams of up to 3300 mm depth. It was further shown that not only the beam depth influences the characteristic bending strength but also the beam length. The size effect,

https://doi.org/10.52202/069179-0063

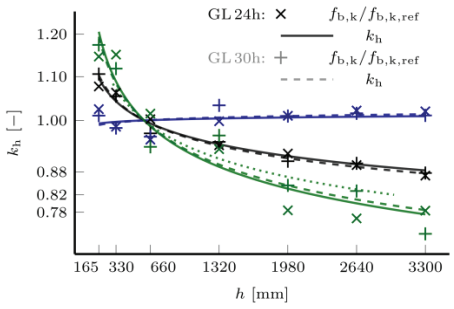

Figure 11: *Size effect k_h according to Eq. (3) based on three different global failure criteria: (i) the load drop criterion in black, (ii) the system stiffness reduction criterion in blue, and (iii) the first crack initiation in the outermost tensile lamination criterion in green compared to (iv) the proposed result by Frese and Blaß [10] with the dotted line in green. [14]*

including changes in beam length and depth, could adequately be described by the concept proposed by Colling [6], at least for beams with depths greater than 660 mm. Additionally, results of numerical studies from the literature could be reproduced by using corresponding global failure criteria.

Numerical simulations offer an efficient way to perform extensive parameter studies of different kinds to make reasonable predictions. Nevertheless, simulation results need to be carefully validated as they might heavily depend on their modelling strategy. Experimental testing of such large GLT beams is unfortunately missing, which would strengthen the value of such studies.

As for future research focus, the aim is to obtain section-wise constant fracture energies for individual knot sections, which then can be used to replace the for now constant one. This could be achieved by employing the so-called phase-field method [25, 26], which is one of our main current research focuses.

ACKNOWLEDGEMENT

The authors gratefully acknowledged the funding from the Austrian Science Fund (FWF) through START grant Y1093 “Virtual Wood Labs” and SFB F77 “Advanced Computational Design”.

REFERENCES

[1] DIN EN 408: Holzbauwerke – Bauholz für tragende Zwecke Und Brettschichtholz – Bestimmung einiger physikalischer und mechanischer Eigenschaften; Deutsche Fassung EN 408:2010+A1:2012. Berlin, Germany: DIN, 2012.

[2] DIN EN 1995-1-1: Eurocode 5: Bemessung und Konstruktion von Holzbauten – Teil 1-1: Allgemeines – Allgemeine Regeln und Regeln für den Hochbau; Deutsche Fassung EN 1995-1-1:2004 + AC:2006 + A1:2008. Berlin, Germany: DIN, 2010.

[3] DIN EN 14080: Holzbauwerke – Brettschichtholz und Balkenschichtholz – Anforderungen; Deutsche Fassung EN 14080:2013. Berlin, Germany: DIN, 2013.

[4] B. Bohannan: Effect of Size on Bending Strength of Wood Members. Research Paper FPL-56. Madison, WI: U.S. Department of Agriculture, Forest Service, Forest Products Laboratory, 1966.

[5] Weibull, W.: A Statistical Theory of the Strength of Materials. Handlingar Nr. 151. Stockholm, Sweden: Ingeniörsvetenskapsakademiens, Generalstabens litografiska anstalts förlag, 1939.

[6] F. Colling: Einfluß des Volumens und der Spannungsverteilung auf die Festigkeit eines Rechteckträgers: Herleitung einer allgemeinen Beziehung mit Hilfe der 2-parametrigen Weibull-Verteilung. *Holz Als Roh- Und Werkstoff*, 44(4):121–125, 1986. doi:10.1007/BF02612013

[7] E. Aasheim, K. H. Solli: Size Factor of Norwegian Glued Laminated Beams. In: *CIB-W18 Meeting 28.* Copenhagen, Denmark, 1995.

[8] G. Kandler, M. Lukacevic, J. Füssl: Experimental Study on Glued Laminated Timber Beams with Well-Known Knot Morphology. *European Journal of Wood and Wood Products*, 76(5):1435–1452, 2018. doi:10.1007/s00107-018-1328-6

[9] G. Schickhofer: Development of Efficient Glued Laminated Timber. In: *CIB-W18 Meeting 29.* Bordeaux, France, 1996.

[10] M. Frese, H. J. Blaß: Numerical Description of Size and Load Configuration Effects in Glulam Structures. In: *Proceedings of the 12th International Conference on Applications of Statistics and Probability in Civil Engineering (ICASP12).* Vancouver, Canada: The University of British Columbia, 2015. doi:10.14288/1.0076135

[11] G. Fink, A. Frangi, J. Kohler: Probabilistic Approach for Modelling the Load-Bearing Capacity of Glued Laminated Timber. *Engineering Structures*, 100:751–762, 2015. doi:10.1016/j.engstruct.2015.06.015

[12] C. Vida, M. Lukacevic, G. Hochreiner, J. Füssl: Size Effect on Bending Strength of Glued Laminated Timber Predicted by a Numerical Simulation Concept Including Discrete Cracking.

Materials & Design, 225:111550, 2023. doi:10.1016/j.matdes.2022.111550

[13] C. Vida, M. Lukacevic, J. Eberhardsteiner, J. Füssl: Modeling Approach to Estimate the Bending Strength and Failure Mechanisms of Glued Laminated Timber Beams. *Engineering Structures*, 255:113862, 2022. doi:10.1016/j.engstruct.2022.113862

[14] C. Vida, M. Lukacevic, G. Hochreiner, J. Füssl: Size Effect of Glued Laminated Timber Predicted by Simulation Concepts – Influence of Global Failure Criterion Definition on Bending Strength and Failure Mechanism. 2023. (manuscript in preparation)

[15] G. Kandler, M. Lukacevic, C. Zechmeister, S. Wolff, J. Füssl: Stochastic Engineering Framework for Timber Structural Elements and Its Application to Glued Laminated Timber Beams. *Construction and Building Materials*, 190(5):573–592, 2018. doi:10.1016/j.conbuildmat.2018.09.129

[16] K. Hofstetter, C. Hellmich, J. Eberhardsteiner: Micromechanical Modeling of Solid-Type and Plate-Type Deformation Patterns within Softwood Materials. A Review and an Improved Approach. *Holzforschung*, 61(4):343–351, 2007. doi:10.1515/HF.2007.058

[17] M. Lukacevic, J. Füssl, J. Eberhardsteiner: Discussion of Common and New Indicating Properties for the Strength Grading of Wooden Boards. *Wood Science and Technology,* 49(3):551–576, 2015. doi:10.1007/s00226-015-0712-1

[18] Abaqus: Abaqus 2021 HF5. Providence, RI, USA, 2021.

[19] Pischl, R.; Schickhofer, G.; Seiner, C.; Steinberger, A.; Gehri, E.; Mauritz, R. (1995). *Entwicklung leistungsfähiger Holzleimbauteile: Zusammenfassender Bericht zum FFF-Forschungsprojekt* (FFF-Forschungsprojekt)Graz/A – Zürich/CH – Wien/A

[20] C. Tapia Camú, S. Aicher: A Stochastic Finite Element Model for Glulam Beams of Hardwoods. *Proceedings of the 2018 World Conference on Timber Engineering (WCTE 2018).* Seoul, Republic of Korea, 2018.

[21] M. Lukacevic, J. Füssl, R. Lampert: Failure Mechanisms of Clear Wood Identified at Wood Cell Level by an Approach Based on the Extended Finite Element Method. *Engineering Fracture Mechanics*, 144:158–175, 2015. doi:10.1016/j.engfracmech.2015.06.066

[22] M. Lukacevic, W. Lederer, J. Füssl: A Microstructure-Based Multisurface Failure Criterion for the Description of Brittle and Ductile Failure Mechanisms of Clear-Wood. *Engineering Fracture Mechanics*, 176:83–99, 2017. doi:10.1016/j.engfracmech.2017.02.020

[23] S. Pech, M. Lukacevic, J. Füssl: A Robust Multisurface Return-Mapping Algorithm and Its Implementation in Abaqus. *Finite Elements in Analysis and Design*, 190:103531, 2021. doi:10.1016/j.finel.2021.103531

[24] M. Frese: *Computergestützte Verfahren zur pragmatischen Beurteilung der Tragwiderstände von Brettschichtholz: Zusammenfassung exemplarischer Simulationsstudien.* Habilitation. Karlsruhe, Germany: KIT Scientific Publishing, 2016.

[25] S. Pech, M. Lukacevic, J. Füssl: A Hybrid Multi-Phase Field Model to Describe Cohesive Failure in Orthotropic Materials, Assessed by Modeling Failure Mechanisms in Wood. *Engineering Fracture Mechanics*, 271:108591, 2022. doi:10.1016/j.engfracmech.2022.108591

[26] S. Pech, M. Lukacevic, J. Füssl: Validation of a hybrid multi-phase field model for fracture of wood. *Engineering Fracture Mechanics*, 275:108819, 2022. doi:10.1016/j.engfracmech.2022.108819

https://doi.org/10.52202/069179-0063